

Quantum chemical calculations and molecular dynamic simulation studies on the corrosion inhibition of aluminium metal by myricetin derivatives

U. Umaru* and A. M. Ayuba

Department of Pure and Industrial Chemistry, Bayero University, Kano, Nigeria

*Corresponding author email: umaruumar80@gmail.com

Received date: May 30, 2020 ; accepted date: Oct. 18, 2020

Abstract

Corrosion inhibition potentials of three myricetin derivatives, myricetin 3-0-alpha rhamnopyranoside (MAP), myricetin 3-0-beta -D-glucopyranoside (MBT) and 4'-methoxy myricetin 3-0-alpha-L-rhamnopyranoside (4MT) on aluminium surface have been studied by quantum chemical calculations and molecular dynamic simulation. Quantum chemical parameters such as E_{HOMO} , E_{LUMO} , ΔE , μ , χ , η , σ and fraction of electron transferred from inhibitor molecule to aluminium metal (ΔN) have been calculated and used to predict the inhibition efficiency of the inhibitor molecules. Local reactivity of the molecules have been analysed by means of Fukui indices. Nevertheless, adsorption interaction of the molecules with aluminium (110) surface was analysed by force quench molecular dynamic simulation. HOMO and LUMO distribution together with local reactivity of the molecules indicated that the active regions of the molecules are located on myricetin ring and hydroxyl (OH) group of the molecules. The molecular dynamic simulation shows that the values of the adsorption energies are negatively less than 100Kcal/mol which indicates a strong physisorption of the molecules onto the aluminium surface. By considering all the studied quantum chemical parameters and the values of adsorption energy obtained from molecular dynamic simulation, a trend could be inferred in terms of inhibition efficiency of the molecules as 4MT>MAP>MBT.

Keywords: Aluminium; corrosion inhibition; myricetin derivatives; quantum chemical parameters; molecular dynamic simulation

1. Introduction

Aluminium metal and its alloys possess high technological importance and industrial applications which include automobiles, household appliances, aviation, containers and electronic devices [1]. The most important feature of aluminium is the formation of protective film oxide on its surface for corrosive immunity in various environments, however the surface dissolves in high concentrations of acid due to the amphoteric nature of the film oxide [2-3]. The use of acid and base solutions in several industrial applications such as acid pickling, oil acidification, acid cleaning, petrochemical industries are very common [4], therefore aluminium metal and its alloys are subject to corrosion. Among several and widely used methods to prevent the corrosion of metals, the most effective and economic method is to dissolve inhibitors in acid solutions [5-6]. In this context development of low cost and easy-to-make organic inhibitors is highly recommended [7].

The most effective inhibitors are the aliphatic or aromatic compounds possessing heteroatoms such as oxygen, nitrogen and sulphur in their molecules [8]. Also, aromaticity, electron density at donor atoms, presence of functional groups like CHO, R=R, R-OH e.t.c facilitates the adsorption of inhibitor molecules on metal surfaces [9]. The traditional methods of testing inhibition efficiencies of inhibitors are weight loss, polarization curves and electrochemical impedance spectroscopy, however these are expensive and time consuming [10]. In view of the above, the use of computational studies such as Quantum chemical calculations and molecular dynamic simulations that uses theoretical chemistry to correlate the inhibition efficiency of inhibitors with their molecular properties is highly recommended [11]. Recently Quantum chemical calculations are used to analyze the interactions between inhibitor molecules and metal surfaces [12]. In general some of the quantum chemical parameters calculated include highest occupied molecular orbital (E_{HOMO}), the lowest

unoccupied molecular orbital (E_{LUMO}), separation energy (ΔE), dipole moment (μ), and those parameters that give information about the reactive behavior such as electronegativity (χ), ionization potential (I), hardness (η), softness (σ), and fraction of electrons transferred from the inhibitor molecule to metal surface (ΔN) [13]. The above parameters are used to obtain the inhibition efficiency of inhibitor molecules in many cases [14-15]. Quantum chemical calculations alone are not enough to study the interaction between inhibitor molecules and metal surfaces [16-17], therefore there is need for experimental modelling for visualization of the interaction between the inhibitor molecules and metal surface [4]. Molecular dynamic simulation can provide the actual interfacial configuration and binding energy between the inhibitors and the metal surface [18]. The aim of this present work is to study the inhibition potentials of 3 myricetin derivatives namely: Myricetin 3-O- α -rhamnopyranoside (MAP), Myricetin 3-O- β -D-glucopyranoside (MBT), and 4'-methoxy-myricetin 3- α -L-rhamnopyranoside (4MT) on aluminium metal and correlate their inhibition efficiencies with quantum chemical parameters without any wet chemical experimentation. This can be achieved by executing quantum chemical calculations and molecular dynamic simulations.

2. Computational Methods

2.1. Quantum Chemical Parameters

Quantum chemical calculations were performed with density functional theory (DFT) programs in DMol3 as contained in the Materials Studio 7.0 software (Accelrys, Inc.) using B3LYP method. DFT has been found to be successful in providing insights into chemical reactivity and selectivity, in terms of global parameters such as electronegativity (χ), hardness (η), and softness (σ), and local ones such as the Fukui function $f(r)$ and local softness $s(r)$. Thus, for an N-electron system with total electronic energy E and an external potential $v(r)$, the chemical potential μ , known as the negative of the electronegativity χ , has been defined as the first derivative of E with respect to N at constant $v(r)$ as in equation (1) [19-23]:

$$\chi = -\mu = -\left(\frac{\partial E}{\partial N}\right)_{v(r)} \quad (1)$$

Hardness (η) has been defined within DFT as the second derivative of E with respect to N at constant $v(r)$ as in equation (2) [19-20, 23-25]:

$$\eta = \left(\frac{\partial^2 E}{\partial N^2}\right)_{v(r)} = \left(\frac{\partial \mu}{\partial N}\right)_{v(r)} \quad (2)$$

Electron affinity (I) and ionization potential (A) are related in turn to the energy of the highest occupied molecular orbital (E_{HOMO}) and of the lowest unoccupied molecular orbital (E_{LUMO}) using the equations (3) and (4) [20-23, 25]:

$$I = -E_{HOMO} \quad (3)$$

$$A = -E_{LUMO} \quad (4)$$

These quantities are also related to the electron affinity (A) and ionization potential (I) using equations (5) and (6)

$$\chi = \frac{(I+A)}{2} = -\frac{E_{LUMO}+E_{HOMO}}{2} \quad (5)$$

$$\eta = \left(\frac{I-A}{2}\right) = -\frac{E_{LUMO}-E_{HOMO}}{2} \quad (6)$$

Global softness can also be defined in equation (7) as [21-22]:

$$\sigma = 1/\eta \quad (7)$$

The local reactivities of the molecules were analyzed through evaluation of the Fukui indices [26]. The Fukui indices are measures of chemical reactivity, as well as an indicative of the reactive regions and the nucleophilic and electrophilic behavior of the molecule. Regions of a molecule where the Fukui function is large are chemically softer than regions where the Fukui function is small, and by invoking the hard and soft acids and bases (HSAB) principle in a local sense, one may establish the behavior of the different sites with respect to hard or soft reagents. The Fukui function $f(r)$ is defined as the first derivative of the electronic density $q(r)$ with respect to the number of electrons N at constant external potential $v(r)$. Thus, using a scheme of finite difference approximations from Mulliken population analysis of atoms in the molecules and depending on the direction of electron transfer, we have equations (8), (9) and (10) [21, 27-28].

$$f_k^+ = q_k(N+1) - q_k(N) \quad (\text{for nucleophilic attack}) \quad (8)$$

$$f_k^- = q_k(N) - q_k(N-1) \quad (\text{for electrophilic attack}) \quad (9)$$

$$f_k^o = \frac{q_k(N+1) - q_k(N-1)}{2} \quad (\text{for radical attack}) \quad (10)$$

Where q_k is the gross charge of atom k in the molecule that is the electron density at a point r in space around the molecule. N corresponds to the number of electrons in the molecule. $N + 1$ corresponds to an anion, with an electron added to the LUMO of the neutral molecule; $N - 1$ corresponds to the cation with an electron removed from the HOMO of the neutral molecule. All calculations were done at the ground state geometry. These functions were condensed to the nuclei by using an atomic charge

partitioning scheme, such as Mulliken population analysis in equations (8-10).

2.2. Molecular Dynamic Simulation

Molecular dynamic simulation was performed by Materials Studio 7.0 software (Accelrys, Inc.) and the optimized structures of the molecules and the Al surface were used for the simulation. Al (1 1 0) was used for the simulation because it is the most densely packed and also the most stable [10, 28-29]. Adsorption of each molecule on the metal surface was analyzed at a molecular level by MD simulations, using Forcite quench MD simulation to sample many different low-energy configurations and identify the low-energy minima [11]. Calculations were carried out using the COMPASS force field and the Smart

algorithm in a simulation box $30 \text{ \AA} \times 25 \text{ \AA} \times 29 \text{ \AA}$ with periodic boundary conditions to model a representative part of the interface, devoid of arbitrary boundary effects. The box composed of the Al slab, cleaved along the (1 1 0) plane, and a vacuum layer of 20 \AA height. The geometry of the bottom layer of the slab was constrained to the bulk positions, whereas other degrees of freedom were relaxed before optimizing the Al(1 1 0) surface, which was subsequently enlarged into a different dimensions of supercell. The molecules were adsorbed on one side of the slab. Temperature was fixed at 350 K, with NVE (microcanonical) ensemble, with a time step of 1 fs and simulation time 5 ps. The system was quenched every 250 steps.

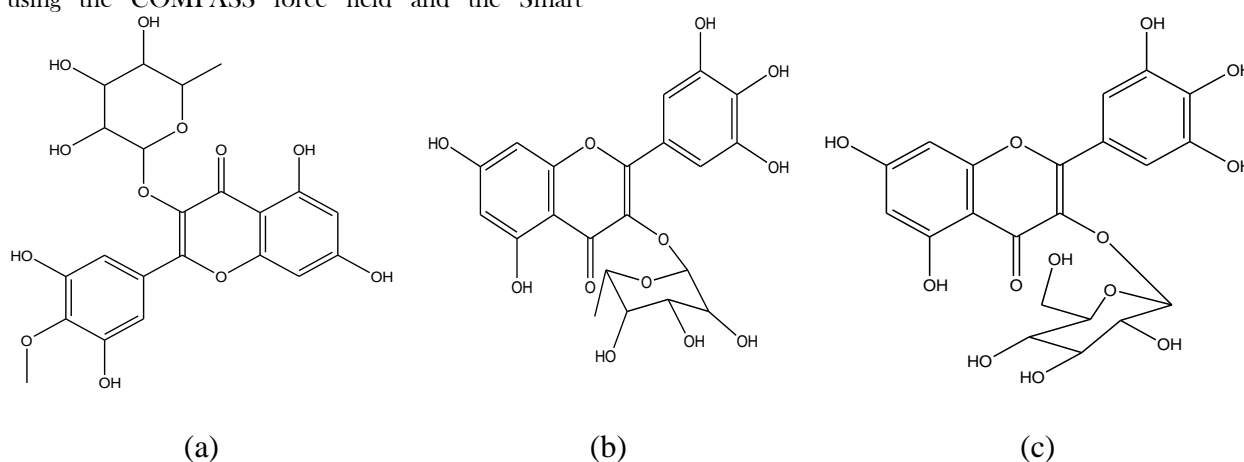


Figure 1. Chemical structures of the studied molecules: (a) Myricetin 3-O- α -rhamnopyranoside (MAP) (b) Myricetin 3-O- β -D-glucopyranoside (MBT) (c) 4'-methoxy-myricetin 3- α -L-rhamnopyranoside (4MT)

3. Results and Discussion

3.1. Frontier Molecular Orbitals

The HOMO region measures the electron donating ability of the molecule to the metal surface while the LUMO region measures the capability of the molecule to accept electrons from the d-orbital of the metal by back bonding [11]. Figures (2-4) show the optimized molecules, HOMO, LUMO and electron density distribution around the studied molecules. It is visible from the figure that both HOMO and LUMO are distributed mainly on the myricetin rings for all the three molecules, this indicates that the myricetin rings and its functional groups (OH) are the centers for the donation of electrons to the empty d-orbitals of the metal as well as accepting electrons from the metal through antibonding orbitals. From the geometry

optimized molecules (figures 2-4), it is observed that all the three molecules are almost planar in shape. However, in MBT one ring of the myricetin molecule is inclined at an angle with respect to the remaining part of the molecule, therefore the molecule somewhat tilted on the aluminium metal surface which reduces the area of contact between the molecules and the metal surface, consequently low adsorption strength when compared to MAP and 4MT. 4MT and MAP optimized molecules on the other hand are planar and possess parallel orientation on aluminium metal surface, thus the area of contact between the molecules and metal surface is maximum and have better adsorption strength. 4MT optimized molecule is the most planar. In this regard the trend in adsorption energy of the molecules follows $4MT > MAP > MBT$. The electron density is saturated

all around each molecule which also facilitates parallel orientation of the molecules on the aluminium metal surface. Figures 2-4 presents the electronic and structural properties of the three myricetin molecules

with the following descriptions: a) Geometry Optimized b) Total Electron Density c) Highest Occupied Molecular Orbital d) Lowest Unoccupied Molecular Orbital.

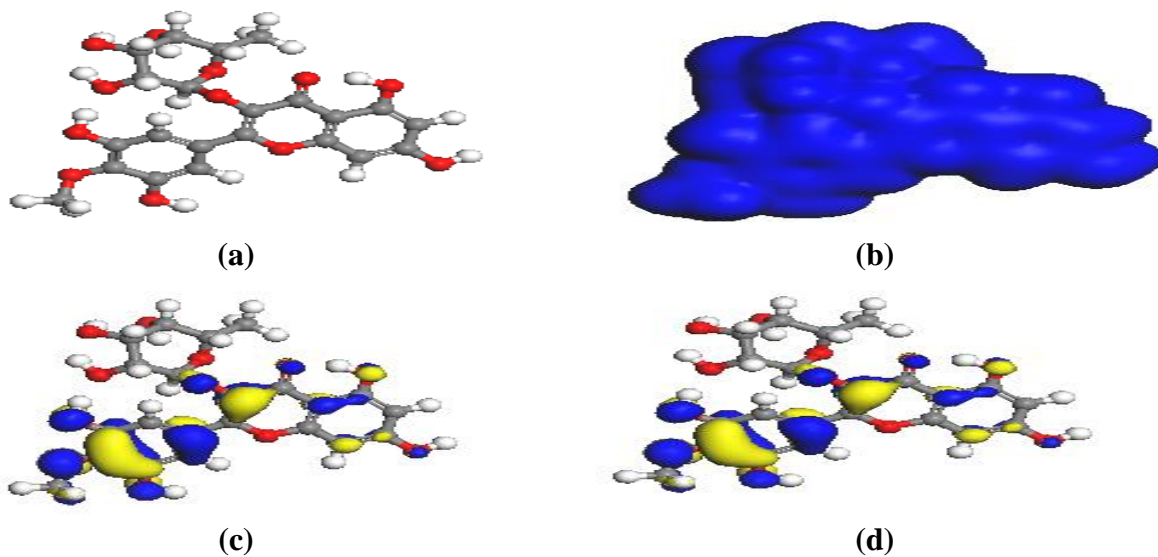


Figure 2. Electronic and Structural Properties of 4MT

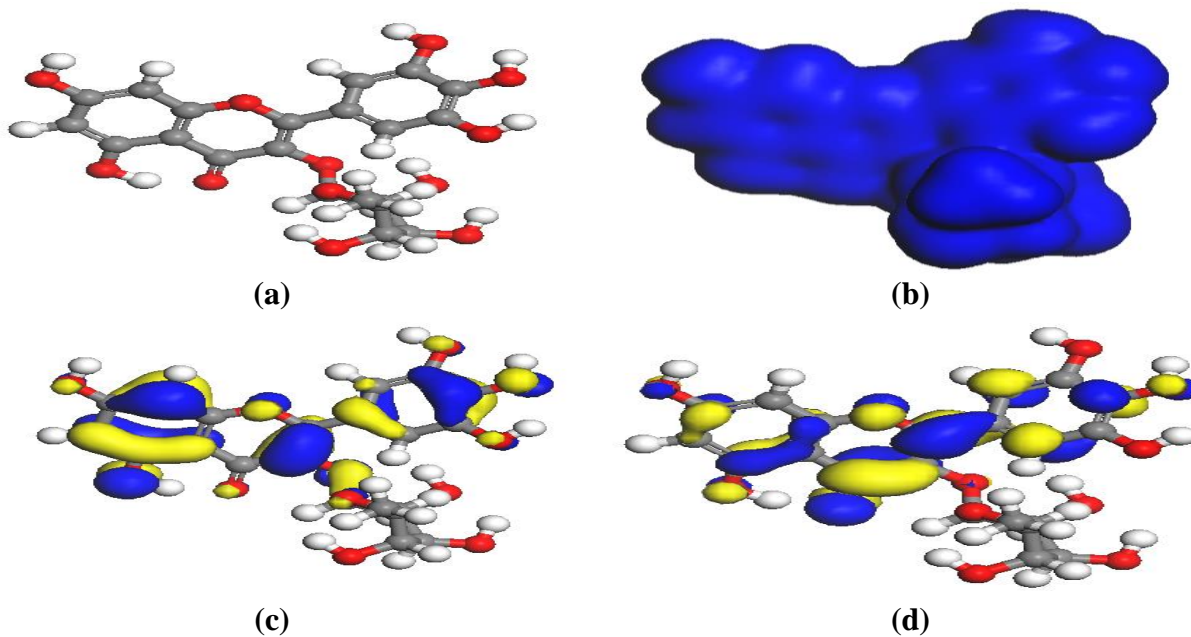


Figure 3. Electronic and Structural Properties of MAP

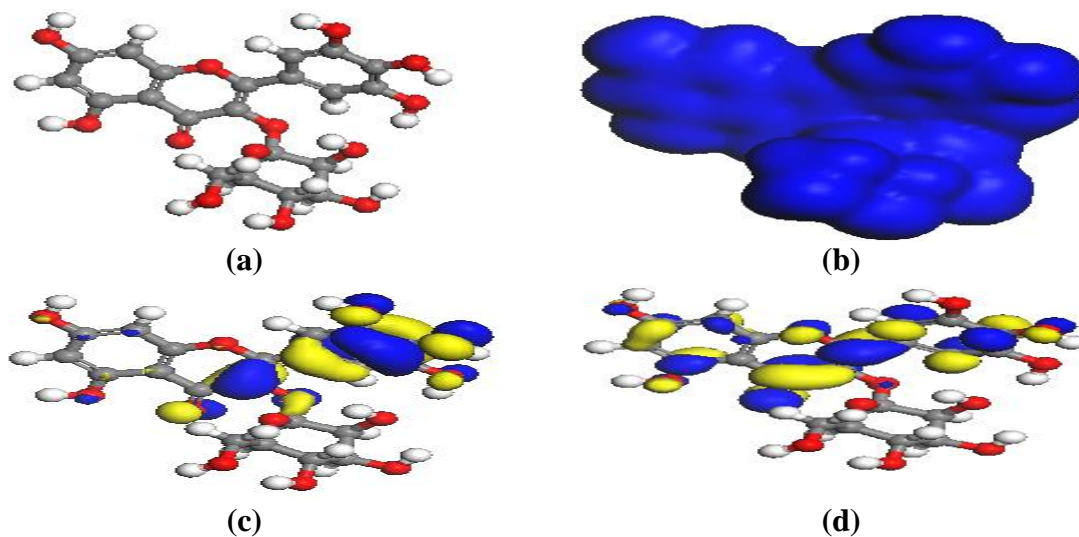


Figure 4. Electronic and Structural Properties of MBT

3.2. Frontier Orbitals Eigen Energies Values

The frontier molecular orbital energies values of the three studied molecules obtained from quantum chemical calculations are presented in table 1. The calculated quantum chemical parameters include: E_{HOMO} , E_{LUMO} , separation energy (ΔE), dipole moment (μ), electronegativity (χ), global hardness (η), global softness (σ) and fraction of electrons transferred from the inhibitor molecule to metal surface (ΔN).

E_{HOMO} is related to the ability of the molecule to donate electrons while E_{LUMO} is associated with the capacity to accept electrons. Higher values of E_{HOMO} reflects a greater tendency of the molecule to donate electrons to other acceptors and the low values of E_{LUMO} shows stronger ability to of accepting electrons [10, 30-31]. From table 1, it is clear that the E_{HOMO} values of inhibitor molecules follow the order 4MT>MAP>MBT while the E_{LUMO} values obey MBT>MAP>4MT. The energy gap (ΔE) between HOMO and LUMO exhibits the ease of the reactivity of the molecules towards the metal surface, the reactivity of the molecules increases as the energy gap decreases since less energy is required to remove an electron from the last occupied molecular orbital [32-33]. The energy gap decreases in the order 4MT>MAP>MBT. Dipole moment (μ) of a molecule is the product of charge and distance between two concerned atoms and is related to the polarity of the polar covalent bonds [4]. There are a lot of disagreements in the literature in correlating dipole moment with inhibition efficiency of the inhibitor molecules [33-35]. In this study, the inhibition efficiency is expected to increases as the dipole moment decreases.

The fraction of electron transferred from the molecules to the aluminium metal surface (ΔN) was calculated as follows

$$\Delta N = \frac{\chi_{Al} - \chi_{inh}}{2(\eta_{Al} + \eta_{inh})} \quad (11)$$

Whereby the difference in electronegativity, ($\chi_{Al} - \chi_{inh}$) drives the electron transfer and the sum of the hardness parameters, ($\eta_{Al} + \eta_{inh}$) act as the resistance. A theoretical value of electronegativity and hardness of bulk aluminium are $\chi_{Al} = 5.60\text{eV}$ and $\eta_{Al} = 0$ respectively by assuming that for a metallic bulk $I = A$ [36-37] because they are softer than neutral metallic atoms. Electron transfer will occur from molecule to metal surface if $\Delta N > 0$ and vice versa if $\Delta N < 0$ [16-17]. Also according to Sastri and Pesumareddi (1997), if ΔN is less than 3.6 inhibition efficiency increases with increasing value of electron donating ability of the molecules while value of ΔN greater than 3.6 indicates a decrease in inhibition efficiency with increasing donating ability of the molecules [38].

Table 1 shows the values of the calculated ΔN for the three molecules, it can be seen that all the three values are positive and are less than 3.6, indicating that electron transfer can occur between the molecules and the metal surface and the inhibition efficiency of the molecules is directly proportional to the electron donating ability of the molecules. The trend observed in terms of electron transfer (table1) was 4MT>MAP>MBT. This is in agreement with the results obtained from previous parameters earlier discussed.

The bonding propensity of inhibitor molecules towards the metal surface has been explained by

HSAB (Hard-Soft-Acid-Base) which suggests that hard acid prefers to bond to hard base and soft acid prefers to bond to soft base [2]. Metal atoms are known to be soft acids, therefore soft base inhibitors are more effective for the metals, thus inhibition efficiency of

the inhibitor molecules increases with increasing softness. By considering the values of softness of the inhibitor molecules (table1), it can be seen that the inhibition efficiency of the molecules is in line with other parameters discussed (4MT>MAP>MBT).

Table 1: Computed Quantum Chemical Parameters (Electronic and Structural) of the Studied Inhibitor Molecules

Properties	Molecules		
	4MT	MAP	MBT
HOMO (at orbital number)	125	121	125
LUMO (at orbital number)	126	122	126
EHOMO (eV)	-4.838	-4.877	-5.180
ELUMO (eV)	-2.65	-2.552	-2.288
ΔE (eV)	2.188	2.325	2.892
Dipole moment (Debye)	2.430	2.513	3.102
Ionization potential (I) (eV)	4.838	4.877	5.180
Electron affinity (A) (eV)	2.650	2.552	2.288
Global hardness (η)	1.094	1.163	1.446
Global softness (σ)	0.914	0.860	0.692
Absolute electronegativity (χ)	3.744	3.715	3.734
Fraction of Electrons Transferred (ΔN)	0.848	0.810	0.487

3.3. Fukui Indices and Local Reactivity

In order to assess the reactive centers of the molecules with respect to electrophilic and nucleophilic attack, local reactivity of each molecule has been analysed by means of Fukui indices. F^- measures reactivity with respect to nucleophilic attack or the capacity to release electron, while F^+ measures reactivity with respect to electrophilic attack or the tendency to accept electrons. The calculated Fukui indices for individual atoms of each molecule are presented in table 2, however, the actual site that is responsible for electrophilic and nucleophilic attack is located on atom possessing the highest absolute value of F^- and F^+ respectively. It can be observed from table 2 that for MBT, according to both Mulliken and Hirshfield, the site for nucleophilic attack is located on O(23) of the myricetin ring which has the highest absolute value (0.089 for Mulliken and 0.087 for Hirshfield) whereas, the electrophilic attack is on O(20) of the OH which bears the highest absolute

value (0.093 for Mulliken and 0.088 for Hirshfield). For 4MT, the nucleophilic center is at C(1) on the myricetin ring with the highest absolute value (0.078 for Mulliken and 0.069 for Hirshfield) while the electrophilic attack is centered at O(31) of the OH group (0.074 for Mulliken and 0.073 for Hirshfield). In MAP molecule nucleophilic site is on O(23) of the carbonyl (C=O) which possesses the highest absolute value (0.054 for both Mulliken and Hirshfield), the electrophilic site is on O(18) of the OH group (0.072 for Mulliken and 0.067 for Hirshfield).

Based on the above explanation it can be observed that in all the three inhibitor molecules, the nucleophilic site is within the myricetin backbone while the electrophilic site is restricted within the oxygen atom of the OH group due to its electron rich character, this is again within the myricetin ring functional group. The above result is in agreement with the results obtained from the distribution of HOMO and LUMO orbitals.

Table 2: Calculated Fukui Indices for the Studied Inhibitor Molecules

Molecule	Nucleophilic (F^-)				Electrophilic (F^+)			
	Mulliken		Hirshfield		Mulliken		Hirshfield	
	Atom	Value	Atom	Value	Atom	Value	Atom	Value
MBT	O(23)	0.089	O(23)	0.087	O(20)	0.093	O(20)	0.088
4MT	C(1)	0.078	C(1)	0.069	O(31)	0.074	O(31)	0.073
MAP	O(23)	0.054	O(23)	0.054	O(18)	0.072	O(18)	0.067

3.4. Molecular Dynamic Simulation

In order to investigate the adsorption behavior of the studied inhibitor molecules on Al (110) surface, molecular dynamic simulations are executed to analyze the interaction of the molecules on Al (110) surface through Forcite quench dynamics. Geometry optimized structure of the molecules were used for the simulation where the atomic coordinates are adjusted based on COMPASS forcefield until and unless the total energy of the structures reach minimum value. The values of E_{total} , $E_{inhibitor}$ and $E_{surface}$ were calculated after the system reaches an equilibrium

(when temperature and energy are balanced). The temperature and energy fluctuation curves for the molecules are shown in figures (5-7). It is clear from the figures that the system tends to equilibrium. The adsorption energies were calculated according to equation (12):

$$E_{adsorption} = E_{total} - (E_{inhibitor} + E_{surface}) \quad (12)$$

Figures 5-7 show adsorption and energy properties of the molecules obtained from forcite quench molecular dynamic simulation: a) side view snapshot b) top view snapshot c) Energy fluctuation curve d) Temperature equilibrium curve

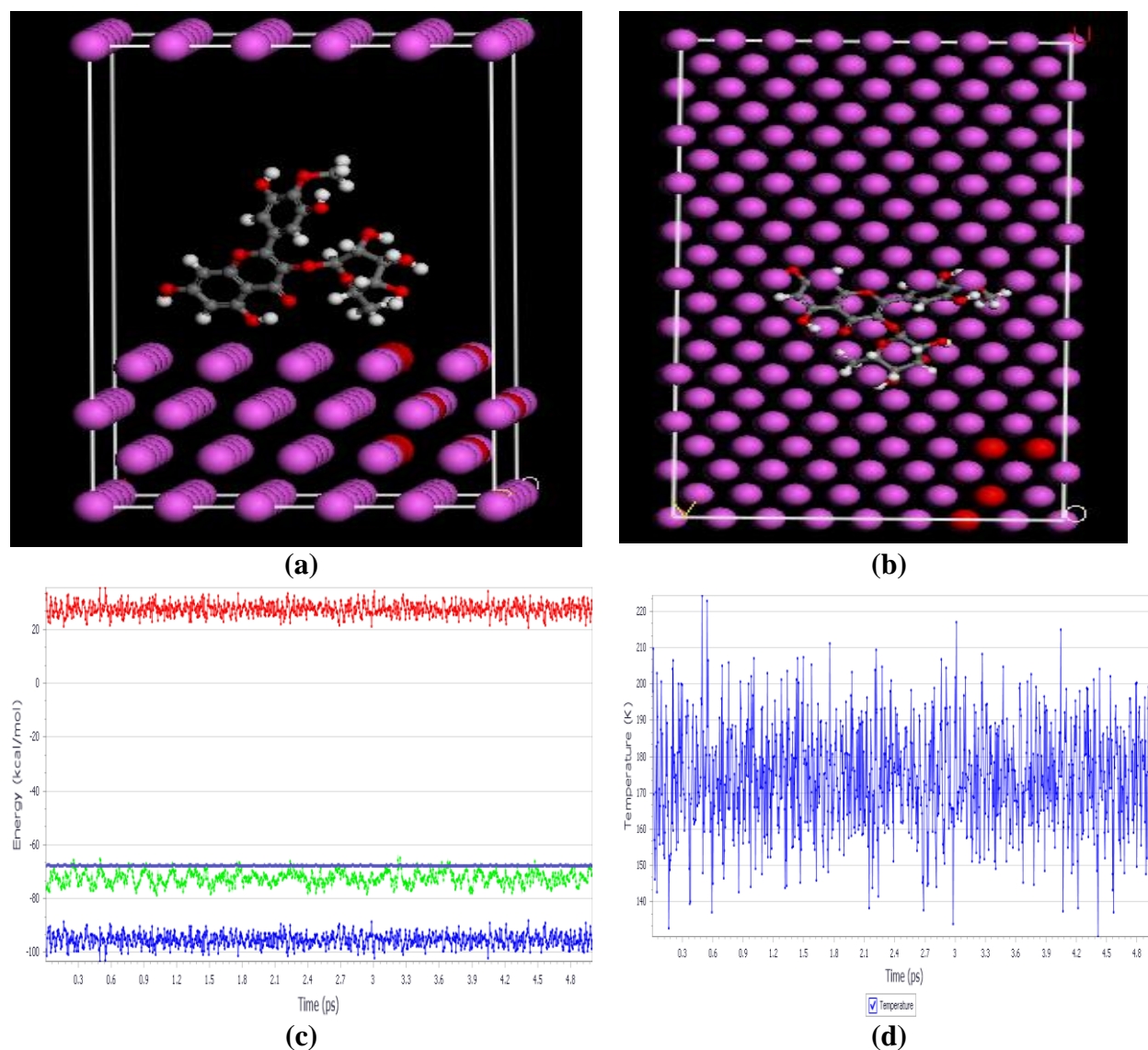


Figure 5. Adsorption and energy properties of 4MT obtained from MD Simulation

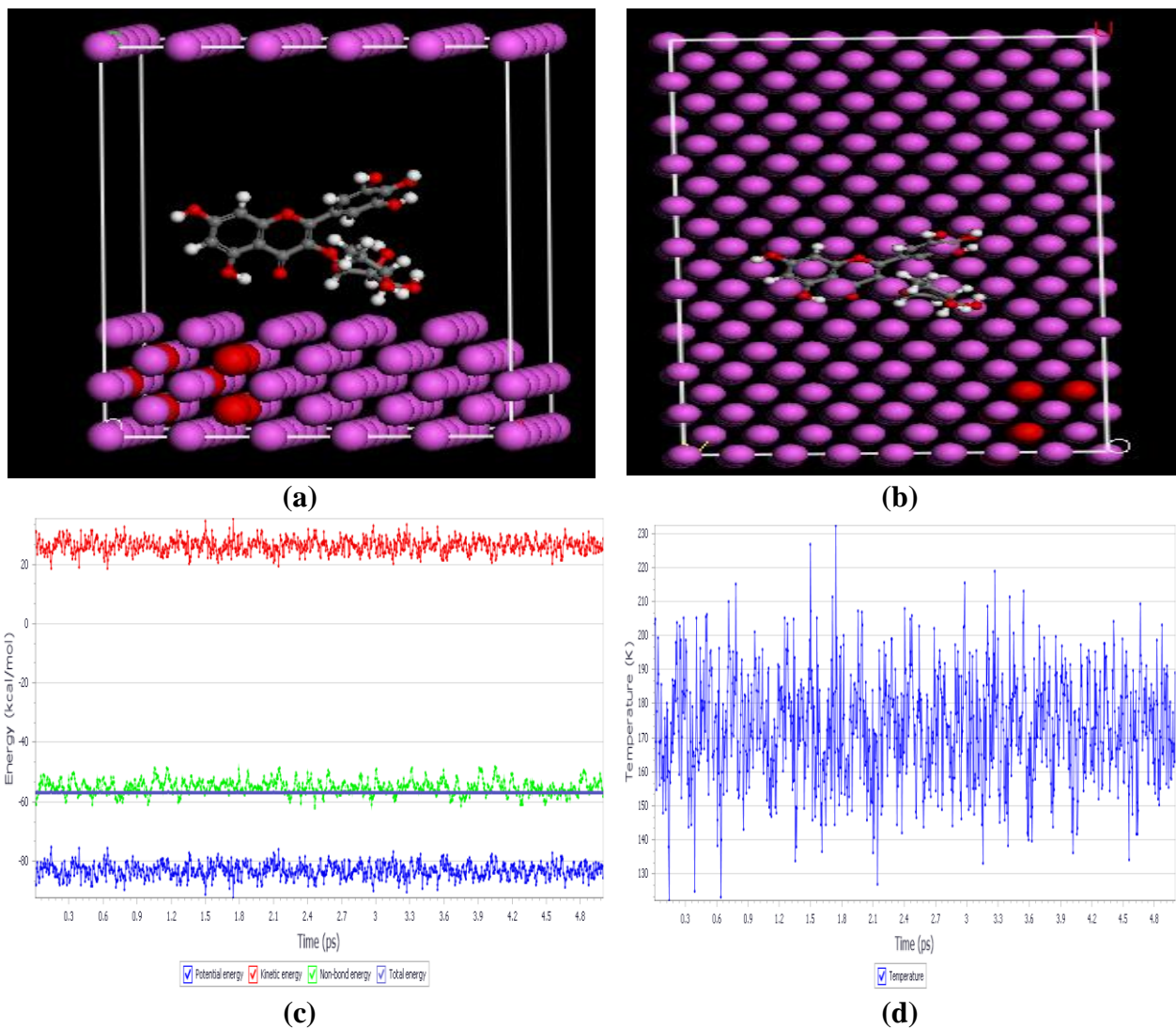


Figure 6. Adsorption and energy properties of MAP obtained from MD Simulation

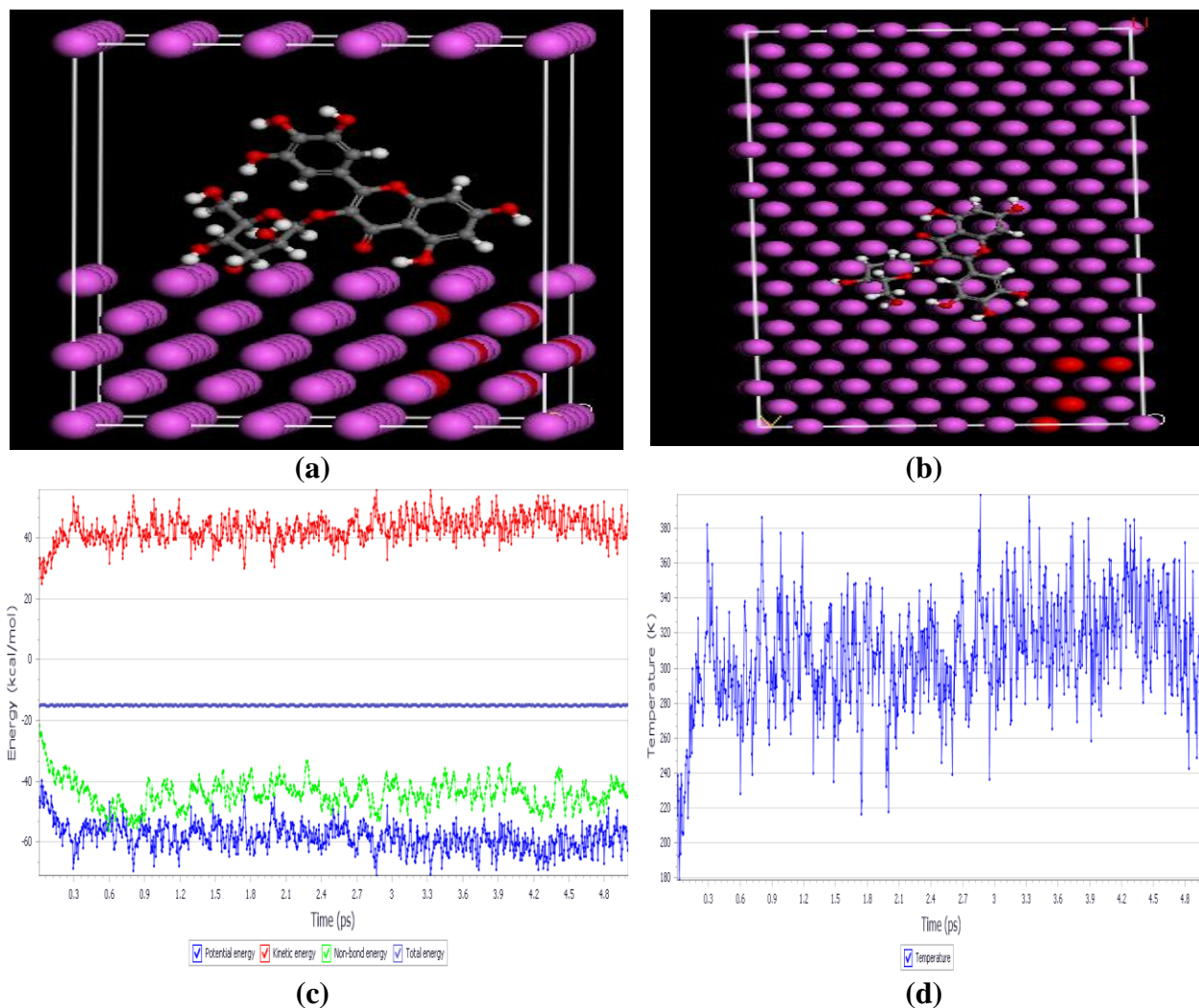


Figure 7. Adsorption and energy properties of 4MT obtained from MD Simulation

Figures (5-7) show the representative snapshots of the top and side view (inset) of the lowest energy adsorption configurations for single molecule of the inhibitors on Al (110) surface from the simulations. Each molecule is observed to maintain a flat-laying (parallel) orientation on the Al (110) surface as

expected from the distribution of electron density all around each molecule. This orientation results to disposition of large surface area on the Al (110) surface for interaction with the molecules and thus higher inhibition efficiency is expected as observed accordingly.

Table 3: Calculated Adsorption Parameters for the Interaction of the Studied Molecules with the Al (110) Surface Using Forcite Quench Dynamics

Properties	Molecules		
	4MT	MAP	MBT
Total Potential Energy (kcal/mol)	-129.799	-120.709	-105.576
Energy of Molecule (kcal/mol)	-58.457	-54.834	-50.012
Energy of Al (110) Surface (kcal/mol)	0.000	0.000	0.000
Adsorption Energy (kcal/mol)	-71.342	-65.875	-55.564

The calculated adsorption energies of the molecules are -71.342 for 4MT, -65.875 for MAP and -55.564 kcal/mol for MBT respectively. The large negative values of the binding energies can be attributed to strong adsorption of the molecules on Al (110) surface [39]. The magnitude of the calculated adsorption energies are all negatively less than 100Kcalmol⁻¹ which is reported by John and Joseph (2013) to be within the range of physical adsorption[2]. The more negative the adsorption energy of the inhibitor-metal surface is, the more the adsorption energy of the inhibitors onto the metal surface and consequently the better the inhibition efficiency [40]. Therefore the trend in terms of inhibition efficiency of the molecules with respect to binding energy follows: 4MT>MAP>MBT. This trend is in line with the trends obtained from frontier molecular orbitals and frontier orbital energies earlier discussed.

4. Conclusion

Quantum chemical calculation results show that the myricetin ring and OH group are the active sites of the three inhibitor molecules. The adsorption energy of the inhibitor molecules onto the Al(1 1 0) surface obey the order 4MT>MAP>MBT as expected to be observed experimentally. 4MT shows best inhibition efficiency due to its possession of highest number of heteroatoms as well as been the largest molecule, however, MBT is less inhibitive than MAP as a result of steric effect. The molecular dynamic simulation results revealed that all the molecules are adsorbed on Al(1 1 0) surface with planar (MBT is slightly in a tilted) orientation. Based on the above information, there is agreement in results obtained from both quantum chemical calculations and molecular dynamic simulation, therefore it can be concluded quantum chemical calculation along with molecular dynamic simulation can be executed for designing of several potential inhibitors without performing any expensive wet experimental study.

References

- [1] R. Padmalatha, D. Prabhu, Journal of material and environmental science 4(2013) 732.
- [2] J. John, S. A. Joseph, Materials and Corrosion 64(2013) 625.
- [3] M.M. Al-Qahtani, K. F. Khaled, Mater. Chem. Phys. 113(2009) 150.
- [4] P. Banerjee, Kr. S. Sourav, G. Pritam, H. Abhiram, C. M. Naresh, Physica E 66(2015) 332.
- [5] M. Abdallah, Corrosion science 45(2003) 2705.
- [6] M. Lagrenee, B. Mernari, M. Bouanis, M. Traisnel, F. Bentiss, Corrosion science 44(2002) 573.
- [7] H. Ashassi-Sorkhabi, N. Ghalebsaz-Jeddi, F. Hashemzadeh, H. Jahani, Electrochim. Acta 51(2006) 3848.
- [8] K. F. Khaled, Corrosion Science 52(2010) 2905.
- [9] I.B. Obot, N.O. Obi-Egbedi, International Journal of Electrochemical Science 4(2009) 1277.
- [10] H. Zhao, X. Zhang, L. Ji, H. Hu, Q. Li, Corrosion Science 83(2014) 261.
- [11] A. M. Ayuba, A. Uzairu, H. Abba, G. A. Shallangwa, Moroccan Journal of Chemistry 6(2018) 160.
- [12] K. R. Ansari, M. A. Quraishi, A. Singh, Corrosion science 79(2014) 5.
- [13] A. M. Ayuba, A. Uzairu, H. Abba, G. A. Shallangwa, Journal of materials and environmental sciences 9(2018) 3026.
- [14] A. Ehsani, M. G. Mahjani, R. Moshrefi, H. Mostaanzadeha, J. S. Shayehb, RSC Adv. 4(2014) 20031.
- [15] S. John, M. Kuruvilla, A. Joseph, RSC Adv. 3(2013) 8929.
- [16] A. Kokalj, S. Peljhan, M. Finsgar, I. Milosev, J. Am. Chem. Soc. 132(2010) 16657.
- [17] N. Kovacevic, A. Kokalj, Corrosion Science 53(2011) 909.
- [18] M. K. Awad, M. R. Mustafa, M. M. A. Elnga, J. Mol. Struct.(Theochem) 959(2010) 66.
- [19] Abd El-Maksoud, Corrosion science 44(2002) 803.
- [20] N.O. Obi-Egbedi, N.D. Ojo, Journal of Science Research 14(2015) 50.
- [21] T. V. Kumar, J. Makangara, C. Laxmikanth, N. S. Babu, International Journal of Computational and Theoretical Chemistry 4(2016) 1.
- [22] N. O. Eddy, P. O. Ameh, N. B. Essien, Journal of Taibah University for Science 12(2018) 545.
- [23] T. A. Salman, K. F. Al-Azawi, I. M. Mohammed, S. B. Al-Baghdadi, A. A. Al-Amiery, T. S. Gaaz, A. A. Kadhum, Results in Physics 10(2018) 291.
- [24] M. A. Ajmal, M. A. Quraishi, A. S. Mideen, Corrosion science 36(1994) 79.
- [25] C. D. D. Sundari, S. Setiadji, M. A. Ramdhani, A. L. Ivansyah, N. I. T. Widhiasari The 2nd Annual Applied Science and Engineering Conference (AASEC 2017) IOP Publishing IOP Conf. Series, Materials Science and Engineering, 288(2018) 012033.
- [26] W. Yang, R.G. Parr, Proc. Natl. Acad. Sci. USA 82(1985) 6723.

- [27] A.A. Khadom, *Journal of Materials and Environmental Sciences* 8(2017) 1153.
- [28] A. Mishra, C. Verma, V. Srivastava, H. Lgaz, M.A. Quraishi, E.E. Ebenso, M. Chung, *Journal of Bio- and Tribo-Corrosion* 4(2018) 32.
- [29] H. Lgaz, R. Salghi, A. Chaouiki, Shubhalaxmi, S. Jodeh, K.S. Bhat, *Cogent Engineering* 5(2018) 1441585.
- [30] G. Gece, S. Bilgic, *Corros. Sci.* 51(2009) 1876.
- [31] I. Ahmad, R. Prasad, M.A. Quraishi, *Corros. Sci.* 52(2010) 1472.
- [32] R.G. Pearson, *J. Chem. Educ.* 64(1987) 561.
- [33] K.F. Khaled, *Electrochem. Acta* 48(2003) 2493.
- [34] M.A. Quraishi, R. Sardar, *J. Appl. Electrochim.* 33(2003) 1163.
- [35] M. Sahin, G. Gece, F. Karci, S. Bilgic, *J. Appl. Electrochim.* 38(2008) 809.
- [36] M.K. Awad, *Canadian Journal of Chemistry* 91(2013) 283.
- [37] P. Zhao, Q. Liang, Y. Li, *Applied Surface Science* 252(2005) 1596.
- [38] V.S. Sastri, J.R. Perumareddi, *Corros. Sc.* 53(1997) 617.
- [39] A.Y. Musa, A.A.H. Khadhum, A.B. Muhammad, M.S. Takriff, *Corros. Sci.* 52(2010) 3331.
- [40] F.E. Awe, S.O. Idris, M. Abdulwahab, E.E. Oguzie, *Cogent Chemistry* 1(2015) 1.